SIMPLICITY, RIGOR AND RELEVANCE IN FLUID MECHANICS
F.J. Higuera, J. Jiménez and J.M. Vega (Eds.)

THE STRUCTURE OF TURBULENCE NEAR WALLS

Javier Jiménez
ETSI Aeronáuticos, Universidad Politécnica
28040 Madrid, Spain
and
Centre for Turbulence Research, Stanford University
Email: jimenez@torroja.dmt.upm.es
Web page: http://torroja.dmt.upm.es

Abstract. The study of turbulence near walls has experienced a renaissance in the last decade, largely because of the availability of high-quality numerical simulations. The resulting emerging models for the viscous and buffer layers over smooth walls are briefly reviewed. It is shown that these near-wall layers are essentially independent of the outer flow, and that there is a family of numerically-exact nonlinear structures which account for about half of the energy production and dissipation in the layer. The other half can be modelled in terms of the unsteady bursting of those structures. Many of the best-known characteristics of the wall layer, such as the dimensions of the dominant structures, are well predicted by these models. It is also noted that as much as two thirds of the friction coefficient in wall-bounded flows at moderate Reynolds numbers depends on processes below $y^+ = 50$, and that this fraction decays only logarithmically when the Reynolds number increases.

Key words: wall turbulence, nonlinear systems.

1. INTRODUCTION

Many papers dealing with turbulence start with the promise of providing simple models for the flow being considered, but few of them succeed. The present paper claims to be one of the former, but probably will not be one of the latter. Turbulence is a complex phenomenon, and simple explanations to complex systems only tend to make them look more complicated than what they really are. However some aspects of turbulence can be easily explained, and those exceptions, even if the models are imperfect, stand out as reasonably safe grounds on which the complexity of the rest of the phenomenon can be anchored. The Kolmogorov cascade theory is a well-known example[1], and so are the discovery and analysis of coherent structures in free shear flows[2] during the 1970's, and the clarification in the 1990's of the structure of the dissipative scales of the vorticity in isotropic turbulence[3,4]. Since the present book and the present meeting celebrate a scientific life dedicated to clarifying difficult problems, it is appropriate to summarize the progress that has

been recently made in providing simple models for a particular turbulent flow.

Our example will be wall-bounded turbulence, and in particular the thin layer in the immediate vicinity of smooth walls. We will see that this layer, although geometrically negligible when compared with the bulk of the flow, is both technologically and scientifically important, and that the viscous effects due to the nearness of the wall make it relatively easy to understand. The modern study of this region began experimentally[5,6] in the 1970's, and got a strong impulse with the advent of high-quality direct numerical simulations[7] in the late 1980's and in the 1990's. That the present review emphasizes numerical results is partly a personal bias of the author, but it is not altogether arbitrary. The near-wall region is relatively well suited to numerical simulation, and relatively difficult to explore experimentally. Much of the available information is numerical.

This paper is organized as follows. In the next section we define the near-wall layer and outline the classical models for it. In section 3 we review the recent work on equilibrium solutions for wall-bounded shear flows, and how they are related to turbulence, and in section 4 we discuss the evidence for time-dependent bursting. Finally some conclusions are offered.

2. THE STRUCTURE OF NEAR-WALL TURBULENCE

It is well known[8] that wall-bounded turbulence over smooth walls can be described to a good approximation in terms of two sets of scaling parameters. Viscosity is important near the wall, and the length and velocity scales in that region are constructed with the kinematic viscosity ν and with the friction velocity $u_\tau = (\tau_w/\rho)^{1/2}$, based on the shear stress at the wall τ_w, and on the fluid density ρ. Magnitudes expressed in these 'wall units' are denoted by $^+$ superscripts. Note that, if y is the distance to the wall, y^+ is a Reynolds number for the size of the structures. The near-wall layer extends at most[9] to $y^+ = 150$, and it is because of those relatively low values that turbulence near smooth walls is a good candidate for simple modelling.

Far from the wall the velocity also scales with u_τ, but the length scale is the flow thickness h. Between the inner and the outer regions there is an intermediate solution with no length scale, where the mean velocity is given approximately by

$$U^+ = \kappa^{-1} \log y^+ + A. \tag{1}$$

The Kármán constant $\kappa \approx 0.4$ is approximately universal. The intercept constant is $A \approx 5$ for smooth walls, but depends on the details of the near-wall region.

The viscous inner layer is extremely important for the flow as a whole. The ratio between the inner and outer length scales is the friction Reynolds number, h^+, which ranges from 200 for barely turbulent flows to $h^+ = 5 \times 10^5$ for large water pipes. In the latter the near-wall layer is only about 3×10^{-4} times the pipe radius, but it follows from (1) that, even in that case, 40% of the velocity drop takes place below $y^+ = 50$. Turbulence is characterized by the expulsion towards the small scales of the energy dissipation, away from the large energy-containing eddies. In wall-bounded flows that separation occurs not only in scale space for the velocity fluctuations, but also in the shape of the mean velocity profile. The singularities are expelled both from the large scales, and from the centre of the flow towards the wall.

Consider for example the energy balance in a turbulent channel. The energy input is the work of the volumetric flux, $2hU_b$, against the pressure gradient, and

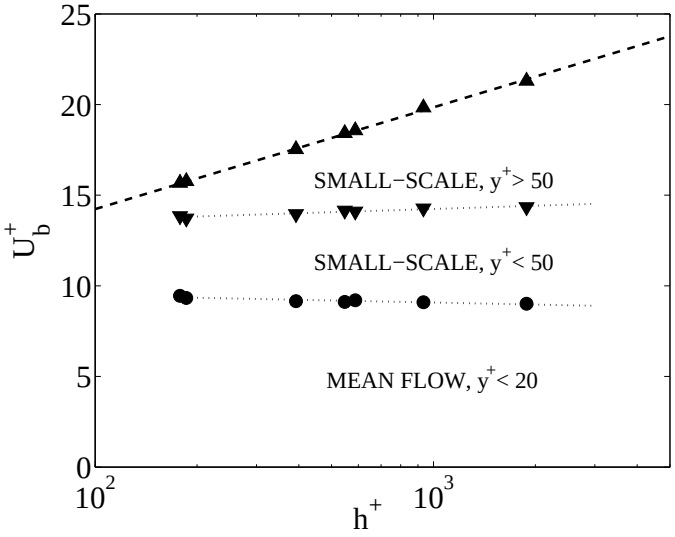

Figure 1. Total energy dissipation by processes below a given wall distance, as a function of Reynolds number. Almost half of the dissipation is due to viscous damping of the mean flow below $y^+ = 20$, and a large part of the rest is due to turbulent fluctuations in the viscous and lower buffer layer. Those two contributions are almost independent of the Reynolds number. The rest is turbulent dissipation in the logarithmic layer, and increases logarithmically with h^+. The upper dashed line is $U_b^+ = \kappa^{-1} \log h^+ + 3$. The two dotted lines are linear fits to aid the eye.

has to balance the total dissipation if the flow is to be statistically stationary. In wall units this is expressed as

$$U_b^+ = \int_0^{h^+} [\varepsilon^+ + (\partial_y U)^{+2}] \, \mathrm{d}y^+, \tag{2}$$

where $\varepsilon = \nu |\nabla \widetilde{u}|^2$ is the 'turbulent' dissipation due to the gradients of the velocity fluctuations $\widetilde{u}$, and the second term of the integral is the dissipation due to the effect of the viscosity on the mean profile. The contributions to (2) from the different parts of the flow are given in figure 1.

In flows away from walls the dissipation due to the mean velocity profile is $O(Re^{-1})$ with respect to the turbulent dissipation, and can be neglected. In wall-bounded flows, figure 1 shows that both contributions are of the same order, although the part due to the mean flow resides almost exclusively below $y^+ = 20$. Most of the turbulent dissipation also happens below $y^+ = 50$.

In the logarithmic layer the dissipation is almost exclusively turbulent, and can be approximated by the local energy production[8]. It can be written as

$$\varepsilon \approx \Pi = -\langle \widetilde{u}\widetilde{v} \rangle \partial_y U = u_\tau^2 (1 - y/h) \partial_y U, \tag{3}$$

where U can be taken from (1) if corrections from the outer 'wake' component are neglected. The dissipation above y_0 is then

$$\int_{y_0^+}^{h^+} \varepsilon^+ \, \mathrm{d}y^+ \approx \kappa^{-1} \log h^+ - \kappa^{-1} (1 + \log y_0^+). \tag{4}$$

If we take $y_0^+ = 50$, as in figure 1, the additive constant in equation (4) is approximately 12, although the experimental value from figure 1 is closer to 11. Only when $h^+ \gtrsim 10^5$ does the logarithmic contribution (3) from the velocity fluctuations in the logarithmic layer begin to be larger than that from the near-wall region.

Integrating the volume flux from equation (1) this constant can be related to the intercept A by

$$A \approx A_{y_0} - \kappa^{-1} \log y_0^+, \tag{5}$$

where A_{y_0} is the value of the integral in (2) in $y = (0,\, y_0)$, and the second summand comes from the additive constant in (4), corrected by the volume flux that would have been obtained by extending (1) from y_0 to the wall. The experimental value $A \approx 5$ is the difference between $A_{50} \approx 14$ and $\kappa^{-1} \log 50 \approx 9$, and therefore depends strongly, through A_{50}, on the near-wall details.

Because of this singular nature, the near-wall layer is not only important for the rest of the flow, but it is also essentially independent from it. That was for example shown by numerical experiments with 'autonomous' simulations[10] in which the outer flow was artificially removed above a certain wall distance δ. The near-wall dynamics were unaffected as long as $\delta^+ \gtrsim 60$.

Understanding the structure of this part of the flow has practical implications. The energy input $U_b^+ = (2/c_f)^{1/2}$ determines the friction coefficient c_f. The relation is inverse; a high normalized dissipation implies low friction, because $\varepsilon^+ = \nu\varepsilon/u_\tau^4$ measures the efficiency of the flow in generating shear stresses for a given energy input. An ideally low-friction turbulent flow would dissipate all its energy without generating Reynolds stresses, and would have $\varepsilon^+ \to \infty$. It follows from figure 1 that any attempt to control wall friction has to centre on the near-wall region, and that only through understanding its mechanics can any such control succeed.

2.1. The classical model

Because of its global influence on the flow, the region below $y^+ \approx 100$ has been intensively studied. It is dominated by coherent streaks of the streamwise velocity and by quasi-streamwise vortices. The former are an irregular array of long ($x^+ \approx 1000$) sinuous alternating streamwise jets superimposed on the mean shear, with an average spanwise separation[11] of the order of $z^+ \approx 100$. The quasi-streamwise vortices are slightly tilted away from the wall[12], and stay in the near-wall region only for $x^+ \approx 200$. Several vortices are associated with each streak[13], with a longitudinal spacing of the order of $x^+ \approx 400$. Most of them merge into disorganized vorticity after leaving the immediate wall neighbourhood[14].

It was proposed very early that streaks and vortices were involved in a mutual regeneration cycle in which the vortices were the results of an instability of the streaks[15], while the streaks were caused by the advection of the mean velocity gradient by the vortices[5,16]. While there is still some discussion on how the vortices are generated, it is known that they derive from the streaks, because disturbing the latter inhibits their formation[10]. That manipulation is only effective if the flow is perturbed below $y^+ \approx 60$, and fails if it is applied only below $y^+ \approx 10$, suggesting that it is predominantly between those two levels that the streaks are involved in the vortex-generation process. There is a substantial body of numerical[17–19] and analytic[20,21] work on the linear instability of model streaks. It shows that streaks are unstable to a variety of sinuous perturbations associated with inflection points of the perturbed velocity profile, whose eigenfunctions correspond well with the shape and location of the observed vortices. The model implied by these instabilities is a time-dependent cycle in which streaks and vortices are created, grow, generate each other, and eventually decay. Reference 10 discusses other unsteady models of this type, and gives additional references.

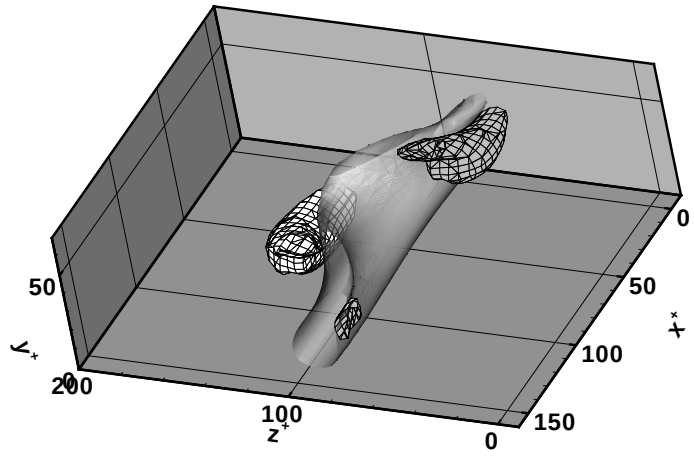

Figure 2. Exact permanent-wave solution for the Navier-Stokes equations in an 'autonomous' domain below $\delta^+ = 40$. The flow is from top-right to bottom-left. The central object is an isosurface of the streamwise velocity, $\widetilde{u}^+ = -3.5$, bounding the streak, and it is flanked by two staggered streamwise vortices of opposite signs, $\omega_x^+ = \pm 0.18$, whose effect is to create an upwash that maintains the streak[26].

3. EXACT SOLUTIONS FOR THE SUBLAYER

A slightly different point of view is that the regeneration cycle is organized around a nonlinear travelling wave, a fixed point in some phase space, which represents a nonuniform streak. This is actually not too different from the previous model, which essentially assumes that the undisturbed streak is a fixed point in phase space, and that the cycle is an approximation to an orbit along its unstable manifold. The new model however considers fixed points which are non-trivially perturbed streaks, and therefore separates the dynamics of turbulence from those of transition.

Nonlinear equilibrium solutions of the three-dimensional Navier–Stokes equations, with characteristics which suggest that they may be useful in such a description, have been obtained numerically in the past few years for plane Couette flow[22,23], plane Poiseuille flow[23–25], and an autonomous wall flow[26]. All those solutions look qualitatively similar[21,27], and take the form of a wavy low-velocity streak flanked by a pair of staggered quasi-streamwise vortices of alternating signs, closely resembling the spatially-coherent objects educed from the near-wall region of true turbulence. An example is shown in figure 2. Their mean and fluctuation intensity profiles are reminiscent of experimental values[23,26], as shown in figure 3. Other properties are also suggestive of real turbulence. For example, the range of spanwise wavelengths in which the nonlinear solutions exist is always in the neighbourhood of the observed spacing of the streaks in the sublayer, $z^+ \approx 100$.

In those cases in which the stability of the equilibrium solutions has been investigated, they have been found to be unstable saddles in phase space at the Reynolds numbers at which turbulence is observed. They are not therefore expected to exist as such in real turbulence, but any turbulent flow could spend a substantial fraction of its lifetime in their neighbourhood. Exact limit cycles and heteroclinic orbits based on these fixed points have been found numerically[28,29], and several reduced dynamical models of the near-wall region have been formulated in terms of low-dimensional projections of such solutions[30–32].

Two questions have to be addressed. The first one is whether all the exact solutions that have been published for wall-bounded flows are related to each other and to near-wall turbulence. The second one is whether real turbulence is best

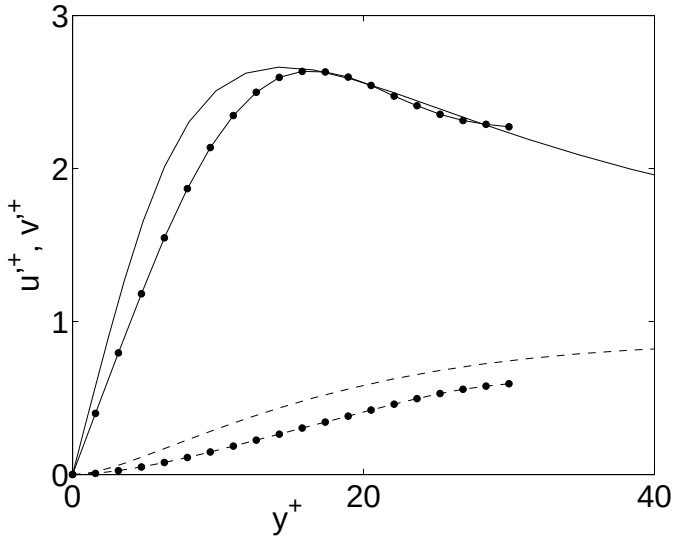

Figure 3. Profiles of the root-mean-square velocity fluctuations in a full channel[7] with $h^+ = 180$ (lines without symbols), and in the permanent-wave autonomous solution in figure 2 (with symbols). ——— , streamwise velocity; - - - - , wall-normal velocity.

described in terms of steady structures or of an unsteady cycle.

The first question is addressed in figure 4. The earliest and best-understood nontrivial steady solutions of a wall-bounded Navier-Stokes shear flow are those by Nagata[22] for a plane Couette flow, which were recently extended by Kawahara[34] to a wider range of parameters. They can be classified into 'upper' and 'lower' branches in terms of their mean wall shear, and both branches have very different profiles of their fluctuation intensities. It can be shown[34] that most of the known wall-bounded solutions by other authors can also be classified into one or the other of Nagata's branches. The 'upper' solutions have relatively weak sinuous streaks flanked by strong vortices. They consequently have relatively weak root-mean-square streamwise-velocity fluctuations u', and strong wall-normal ones v' compared with those in the lower branch. The solution in figure 2 belongs to the upper branch, and we already saw in figure 3 that its r.m.s. velocity-fluctuations profiles agree well with those of a full channel. 'Lower' solutions have stronger and essentially straight streaks, and much weaker vortices.

The relative strength of both types of fluctuations for a particular solution can be characterized by the maximum values of its u' and v' profiles, both of which are usually attained within the near-wall layer. Different solutions can then be compared among themselves, and with fully-turbulent flows, by comparing those two numbers. This is done in figure 4, but the comparison with full turbulence is not straightforward. Statistics compiled over small boxes of different sizes are not comparable, even within the same flow, because they are not 'converged'. In particular the r.m.s. profiles of the exact solutions, which are computed over periodic domains of size $L_x^+ \times L_z^+ \approx 400 \times 100$ parallel to the wall, cannot be compared directly with the standard intensity profiles compiled from full experiments or from computations, which typically have domains of the order of $L_x^+ \times L_z^+ \approx 10,000 \times 5,000$.

To allow the comparison in figure 4, each wall of the large computational boxes is divided into 'minimal' sub-boxes with the same wall-parallel dimensions as the smaller computational boxes of the exact solutions, $b_x^+ \times b_z^+ \approx 380 \times 110$, and the

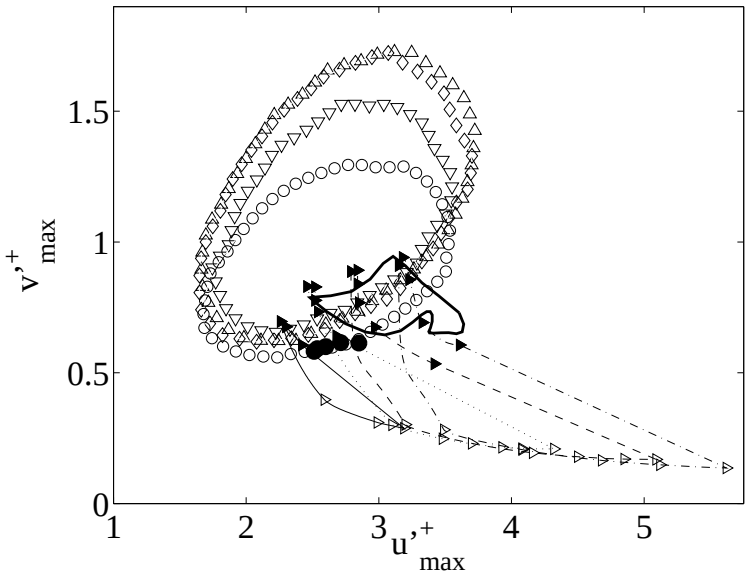

Figure 4. Comparison of some exact solutions with the near-wall turbulent structures, in terms of the maxima of the u' and v' profiles taken over boxes of size $b_x^+ \times b_z^+ \times y^+ = 380 \times 110 \times 50$. $\triangleright$, Nagata's solutions for Couette flow, at different Reynolds numbers[34]. Solid symbols are 'upper branch' solutions, and open ones are 'lower branch'. $\bullet$, autonomous permanent waves[26]. The solid loop is an exact limit cycle in plane Couette flow[28]. Other open symbols are probability isocontours from large-box Poiseuille flows[36,37]: $\triangle$, $h^+ = 1880$; $\Diamond$, 950; $\triangledown$, 550; $\circ$, 180. They contain 90% of the boxes in the p.d.f.

statistics are compiled over them. In addition, each wall of the full channels is treated independently, and the intensity profiles are compiled only from the wall to $y^+ = 50$. Each sub-box is characterized by its maximum r.m.s. intensities, and the values for different sub-boxes are summarized as a joint probability density function of the two quantities, compiled over the different sub-boxes and over time. Each flow is not therefore characterized by a single point, but by the probability distribution of the possible states of the sub-boxes.

The results of the figure suggest that only the 'upper-branch' exact solutions are representative of real turbulence, at least at the scales corresponding to a single streak and to a single vortex pair. They also show that the correspondence is reasonably good, but only for the weaker turbulent fluctuations. Specially for the wall-normal velocities, there are turbulent fluctuations in the near-wall region which are substantially stronger than those of the exact solutions. Note that the probability densities of the turbulent flows depend on the Reynolds number, but that they saturate beyond approximately $h^+ = 1000$. This is not the case for the velocity fluctuation profiles compiled over full flows, which keep increasing for much higher Reynolds numbers[38]. That effect is due to large outer-flow velocity fluctuations reaching the wall[35,36], and is unrelated to the structures being considered here.

The classification of the wall-parallel size of the structures in the near-wall region is shown in figure 5, which contains two-dimensional premultiplied energy spectra of the streamwise velocity, $k_x k_z E_{uu}(k_x, k_z)$, displayed as functions of the wavelengths $\lambda = 2\pi/k$, instead of the wavenumbers k. The three spectra in the figure correspond to an autonomous flow and to two large channels at moderate Reynolds numbers. They differ from each other almost exclusively in the long and wide structures represented in the upper-right corner of the spectrum, whose sizes are of the order of $\lambda_x \times \lambda_z = 10h \times h$. Those spectra are fairly well understood[35,36]. The lower-left cor-

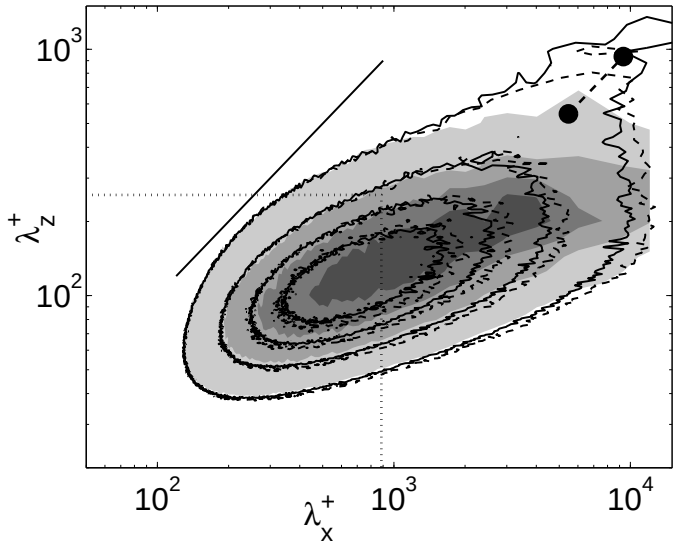

Figure 5. Two-dimensional spectral energy density of the streamwise velocity in the near-wall region ($y^+ = 16$), in terms of the streamwise and spanwise wavelengths. Shaded contours are an autonomous flow[35] whose vorticity fluctuations are masked above $y^+ = 60$. Lines are full channels[37]. ---- , $h^+ = 550$; —— , $h^+ = 940$. The two solid dots are $\lambda_x \times \lambda_z = 10h \times h$ for the two full flows. The solid diagonal line is isotropy, $\lambda_x = \lambda_z$, and the dotted rectangle is the approximate extent of the transfer function of the averaging boxes used in figure 4. Isolines are equispaced from zero to the maximum of the autonomous spectrum.

ner contains the structures discussed in this section, which are very approximately universal and local to the near-wall layer. The anisotropic ridge shared by the three spectra is formed by dynamically-passive wakes of those small active structures. The larger structures in the upper edge of the spectra, and specially those in the top-right corner, extend into the logarithmic and outer layers, scale in outer units, and correspond approximately to the 'attached eddies' proposed by Townsend[39]. Because they are too large to be contained within the averaging boxes used in this section, they do not influence the statistics in figure 4.

4. BURSTING VERSUS STEADY SOLUTIONS

The next question is whether near-wall turbulence is best described by steady or by unsteady solutions. The unsteady models discussed in section 2 follow the original interpretation of the visualizations of the sublayer[5], which was that the streaks regenerate through intermittent 'bursting'. That interpretation has sometimes been dismissed as a visualization artifact, and even the original authors acknowledged that their visualizations could be consistent with advecting permanent objects[33]. Bursting eventually became associated with the ejections observed by stationary velocity probes, specially after numerical simulations showed that the velocity streaks were long-lived. The sweeps and the ejections identified in the analysis of single-point data were then associated to the passing of shorter quasi-streamwise vortices, intermittent in space but not necessarily in time[14]. The question of whether the observed temporally-intermittent sublayer events were artifacts or really existed, was bypassed by this explanation.

The difficulty of following for long times individual structures in fully turbulent flows complicates the experimental or numerical distinction between permanent structures and time-dependent processes with a long period, but intermittent breakdown of near-wall turbulence is observed in minimal-flow numerical simulations[13]

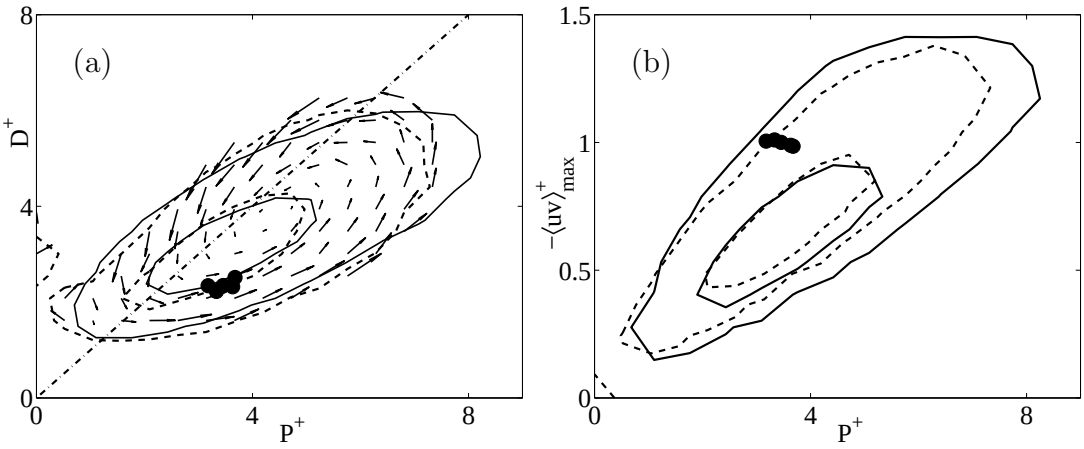

Figure 6. Joint probability density functions of: (a) The turbulent energy production and dissipation, integrated below $y^+ = 35$. The chaindotted diagonal line is energy equilibrium, $P = D$. The arrows are explained in the text. (b) Production below $y^+ = 35$, and the maximum of the Reynolds stress. - - - - , minimal Poiseuille flow, $L_x^+ \times L_z^+ = 450 \times 125$; ——— , full channel, analysed over similar sub-boxes. In both cases, $h^+ \approx 180$, and the probability isolines contain 40% and 90% of the data. The solid circles are as in figure 4.

in which spatial intermittency is not an issue. The same is true of autonomous wall flows in which the observation is simplified by the small wall-normal dimensions of the simulation domain[10].

Minimal channels are numerical simulations in which the wall-parallel periodic dimensions of the computational box are small enough to produce a periodic array of identical essentially-single structures. They are known to approximate well fully-turbulent flows near the wall[13], and they are useful in analysing the dynamics of the flow because their single structures can easily be followed in time. An example is given in figure 6(a), where the evolution of the flow near the wall in a minimal channel is represented in terms of the production and of the dissipation of turbulent energy below $\delta^+ = 50$,

$$P = -\int_0^\delta \langle \tilde{u}\tilde{v} \rangle \, \partial_y U \, \mathrm{d}y, \tag{6}$$

and

$$D = \nu \int_0^\delta \langle |\nabla \tilde{\mathbf{u}}|^2 \rangle \, \mathrm{d}y. \tag{7}$$

The balance of those two quantities determines how energy accumulates or drains from the perturbations. Each instantaneous state of the minimal flow is represented by a point in the (P, D) plane, and the joint p.d.f. in figure 6(a) is compiled as the system evolves in time. The arrows in the figure represent the evolution velocity of the system in parameter space, ($\mathrm{d}P/\mathrm{d}t$, $\mathrm{d}D/\mathrm{d}t$). The p.d.f. is compiled as a histogram over 25×25 bins, and the arrows represent the mean evolution velocity of all the points within a particular bin. These velocities are in general somewhat lower than the true evolution velocities of the individual systems within the bin, because of the effect of the vector averaging, but the mean velocities measured in the bins near the periphery of the distribution are of the same order as their standard deviations over those bins, and they are therefore probably representative of the true values.

The wall region of this minimal flow describes a cycle in the (P, D) plane, during which the fluctuations accumulate energy when $P > D$, grow, cross into the dissipative part of the plane where $D > P$, and finally decay. The period of the cycle is

of the order of $T^+ \approx 400$ in the high-Reynolds number limit[34], which is fairly long. The structures advect about $x^+ = 5000$ during that time[40]. The steady autonomous waves in figure 2 are seen in this representation to be production-dominated and relatively quiescent. They produce extra turbulent energy which they export to the numerically-damped outer region. This behaviour is similar to that of real near-wall turbulence, which exports energy to the outer flow[41]. The Couette limit cycle which was included in figure 4, but which is not plotted here for clarity, is a miniature version of the energy cycle in figure 6(a), with whom it shares many characteristics[34].

Figure 6(a) shows that the minimal flow 'bursts' in the sense of the original unsteady descriptions in reference 5. It is difficult to obtain the same temporal information for full flows, because of the problem of identifying individual structures, but a joint p.d.f. of P and D can be compiled in those cases over minimal sub-boxes, in the same way as above. Such a p.d.f. is included in figure 6(a), and it is similar enough to that of the minimal case to suggest that the full flow is also bursting.

The final question is whether the bursting of the sublayer is important for the flow as a whole. We saw at the beginning of this paper that a large fraction of the total energy dissipation in a channel happens below $y^+ = 50$, and that roughly half of that dissipation is associated with the gradient of the mean velocity profile below $y^+ = 20$. It is interesting to know what fraction of the dissipation is associated with bursts, and how much is due to the quiescent structures. Figure 6(a) cannot be used for that purpose, because the mean flow is not included in (7), but it can be shown that the correlation between the production and the total dissipation is even stronger than for D. If we define 'bursts' from figure 6(a) as points where $P^+ \gtrsim 4$, roughly half of the total dissipation is due to them.

Even more closely related to the friction coefficient than the dissipation is the Reynolds stress averaged over individual boxes. The joint p.d.f of the production and the maximum stress is given in figure 6(b) and, if we again use P as diagnostic for bursting, it is clear that most of the Reynolds stress is associated with unsteady bursting. Note that these bursts are not the ejections associated with the passing of quiescent vortices. The sub-boxes that we have used to analyse the flow are large enough to contain a full vortex pair, and in particular they are large enough for their mean wall-normal velocity to be always very close to zero. The differences of the Reynolds stresses in figure 6(b) are differences between quiescent and excited full sets of structures. Other mean profiles also change according to the location of the sub-box in the bursting cycle[34]. The general effect of bursting is to move the active structures away from the wall.

5. CONCLUSIONS

We have briefly reviewed the present state of the understanding of the dynamics of turbulent flows near smooth walls. This is a subject that, like most others in turbulence, is not completely closed, but which has evolved in the last two decades from empirical observations to relatively coherent theoretical models. It is also one of the first cases in turbulence, perhaps together with the structure of small-scale vorticity in isotropic turbulence, in which the key technique responsible for cracking the problem has been the numerical simulation of the flow. The reason is that the Reynolds numbers of the important structures are low, and therefore accessible to computation, while experiments are difficult. For example the spanwise Reynolds number of the streaks is only of the order of $z^+ = 100$, which is less than

a millimetre in most experiments, but we have seen that it is well predicted by the range of parameters in which the associated equilibrium solutions exit. We have seen that the larger structures coming from the outside flow interfere only weakly with the near-wall region, because the local dynamics are intense enough to be always dominant. The spacing of the streaks just mentioned has been observed up to the highest Reynolds numbers of the atmospheric boundary layer[42].

On the other hand the thinness of the layer in which the dynamics takes place makes the flow very sensitive to small perturbations at the wall. Roughness elements with heights of the order of a few wall units, microns in a large pipe, completely destroy the delicate cycle that has been described here, and can increase the friction coefficient by a factor of two[43]. Conversely it only takes a concentration of polymers of a few parts per million in the near-wall region[44] to decrease the drag coefficient by 40%. The same can be said of the control strategies based on the manipulation of the near-wall structures[45,46]. It has often been questioned whether such strategies, which have mostly been developed in low-Reynolds-number numerical simulations, would lose effectiveness at higher Reynolds numbers. The analysis in section 2 shows that they will, because the dissipation in the logarithmic layer cannot be avoided, but that the degradation with h^+ is only logarithmic. The same conclusion follows from the experience with riblets, another near-wall manipulation method, which are known to remain effective at flight Reynolds numbers[47].

The preparation of this paper was supported in part by the CICYT grant DPI2003–03434. I am deeply indebted to J.C. del Álamo, O. Flores, G. Kawahara and M.P. Simens for providing most of the data used in the figures.

References

[1] Kolmogorov, A.N., The local structure of turbulence in incompressible viscous fluids at very large Reynolds numbers, *Dokl. Akad. Nauk. SSSR* **30**, 299–303 (1941). Reprinted in *Proc. R. Soc. London* **A 434**, 9–13 (1991).

[2] Brown, G.L. and Roshko, A., On the density effects and large structure in turbulent mixing layers, *J. Fluid Mech.* **64**, 775–816 (1974)

[3] Vincent, A. and Meneguzzi, M., On the dynamics of vorticity tubes in homogeneous turbulence, *J. Fluid Mech.* **258**, 245-254 (1994)

[4] Jiménez, J., Wray, A.A., Saffman, P.G. and Rogallo, R.S., The structure of intense vorticity in isotropic turbulence, *J. Fluid Mech.* **255**, 65–90 (1993)

[5] Kim, H.T., Kline, S.J. and Reynolds, W.C., The production of turbulence near a smooth wall in a turbulent boundary layers, *J. Fluid Mech.* **50**, 133–160 (1971)

[6] Morrison, W.R.B., Bullock, K.J. & Kronauer, R.E., Experimental evidence of waves in the sublayer. *J. Fluid Mech.* **47**, 639–656 (1971)

[7] Kim, J., Moin, P. & Moser, R., Turbulence statistics in fully developed channel flow at low Reynolds number. *J. Fluid Mech.* **177**, 133–166 (1987)

[8] Tennekes, H. and Lumley, J.L., *A first course in turbulence*, chapter 8. MIT Press (1972)

[9] Österlund, J.M., Johansson, A.V., Nagib, H.M. & Hites, A note on the overlap region in turbulent boundary layers, *Phys. Fluids* **12**, 1–4 (2000)

[10] Jiménez, J. & Pinelli, A., The autonomous cycle of near wall turbulence, *J. Fluid Mech.* **389**, 335–359 (1999).

[11] Smith, C.R. & Metzler, S.P., The characteristics of low speed streaks in the near wall region of a turbulent boundary layer. *J. Fluid Mech.* **129**, 27–54 (1983)

[12] Jeong, J., Hussain,F., Schoppa,W. & Kim,J., Coherent structures near the wall in a turbulent channel flow. *J. Fluid Mech.* **332**, 185–214 (1997)

[13] Jiménez, J. & Moin, P., The minimal flow unit in near wall turbulence. *J. Fluid Mech.* **225**, 221–240 (1991)

[14] Robinson, S.K., Coherent motions in the turbulent boundary layer. *Ann. Rev. Fluid Mech.* **23**, 601–639 (1991)

[15] Swearingen, J.D. & Blackwelder, R.F., The growth and breakdown of streamwise vortices in the presence of a wall. *J. Fluid Mech.* **182**, 255–290 (1987)

[16] Bakewell, H. P. & Lumley, J. L., Viscous sublayer and adjacent wall region in turbulent pipe flow. *Phys. Fluids* **10**, 1880–1889 (1967)

[17] Hamilton, J. M., Kim, J. & Waleffe, F., Regeneration mechanisms of near-wall turbulence structures. *J. Fluid Mech.* **287**, 317–348 (1995)

[18] Waleffe, F., On a self-sustaining process in shear flows. *Phys. Fluids* **9**, 883–900 (1997)

[19] Schoppa, W. & Hussain, F., Coherent structure generation in near-wall turbulence. *J. Fluid Mech.* **453**, 57–108 (2002)

[20] Reddy, S.C., Schmid, P.J., Baggett, J.S. & Henningson, D.S., On stability of streamwise streaks and transition thresholds in plane channel flows. *J. Fluid Mech.* **365**, 269–303 (1998)

[21] Kawahara, G., Jiménez, J., Uhlmann, M. & Pinelli, A., Linear instability of a corrugated vortex sheet – a model for streak instability, *J. Fluid Mech.* **483** 315–342 (2003)

[22] Nagata, M., Three-dimensional finite-amplitude solutions in plane Couette flow: bifurcation from infinity, *J. Fluid Mech.* **217**, 519–527 (1990).

[23] Waleffe, F., Homotopy of exact coherent structures in plane shear flows, *Phys. Fluids* **15**, 1517–1534 (2003).

[24] Toh, S. & Itano, T., On the regeneration mechanism of turbulence in the channel flow, *Proc. Iutam Symp. on Geometry and Statistics of Turbulence.* (eds. T. Kambe, T. Nakano and T. Muiyauchi), Kluwer. 305–310 (2001)

[25] Waleffe, F., Exact coherent structures in channel flow, *J. Fluid Mech.* **435**, 93-102 (2001).

[26] Jiménez, J. & Simens, M.P., Low-dimensional dynamics in a turbulent wall flow, *J. Fluid Mech.* **435**, 81–91 (2001).

[27] Waleffe, F., Three-dimensional coherent states in plane shear flows. *Phys. Rev. Letters* **81**, 4140–4143 (1998)

[28] Kawahara, G. & Kida, S., Periodic motion embedded in plane Couette turbulence: regeneration cycle and burst, *J. Fluid Mech.* **449**, 291–300 (2001).

[29] Toh, S. & Itano, T., A periodic-like solution in channel flow, *J. Fluid Mech.* **481**, 67–76 (2003)

[30] Aubry, N., Holmes, P., Lumley, J.L. & Stone, E., The dynamics of coherent structures in the wall region of a turbulent boundary layer, *J. Fluid Mech.* **192**, 115–173 (1988)

[31] Sirovich, L. & Zhou, X., Dynamical model of wall-bounded turbulence. *Phys. Rev. Lett.* **72**, 340–343 (1994)

[32] Waleffe, F., On a self-sustaining process in shear flows, *Phys. Fluids* **9**, 883–900 (1997)

[33] Offen, G.R. & Kline, S.J., A proposed model for the bursting process in turbulent boundary layers, *J. Fluid Mech.* **70**, 209–228 (1975)

[34] Jiménez, J., Kawahara, G., Simens, M.P., Nagata, M. & Shiba, M., Characterization of near-wall turbulence in terms of equilibrium and 'bursting' solutions, submitted to *Phys. Fluids*.

[35] Jiménez, J., del Álamo, J.C. & Flores, O., The large-scale dynamics of near-wall turbulence, *J. Fluid Mech.* **505**, 179–199 (2004)

[36] del Álamo, J.C. & Jiménez, J., Spectra of very large anisotropic scales in turbulent channels, *Phys. Fluids* **15** L41–L44 (2003)

[37] del Álamo, J.C., Jiménez, J., Zandonade, P. & Moser, R.D., Scaling of the energy spectra of turbulent channels, *J. Fluid Mech.* **500**, 135–144 (2004)

[38] DeGraaf, D.B. & Eaton, J.K., Reynolds number scaling of the flat-plate turbulent boundary layer, *J. Fluid Mech.* **422**, 319–346. (2000)

[39] Townsend, A. A. *The structure of turbulent shear flows*, 2nd edn. Cambridge U. Press (1976)

[40] Kim, J. & Hussain, F., Propagation velocity of perturbations in channel flow. *Phys. Fluids* A **5**, 695–706 (1993)

[41] Jiménez, J., The physics of wall turbulence, *Physica A* **263**, 252–262 (1998)

[42] Klewicki, J.C., Metzger, M.M., Kelner, E. & Thurlow, E.M., Viscous sublayer flow visualizations at $R_\theta \approx 1,500,000$. *Phys. Fluids* **7**, 857–863 (1995)

[43] Jiménez, J., Turbulent flows over rough walls, *Ann. Rev. Fluid Mech.* **36**, 173–196 (2004)

[44] McComb, W.D. *The physics of fluid turbulence.* Oxford U. Press (1990)

[45] Choi, H., Moin, P. and Kim, J., Active turbulence control and drag reduction in wall-bounded flows. *J. Fluid Mech.* **262**. 75–110 (1994)

[46] Jiménez, J., On the structure and control of near wall turbulence, *Phys. Fluids* **6** 944–953 (1994)

[47] Walsh, M.J. 1990 Riblets, in *Viscous drag reduction in boundary layers*, edited by D.M.Bushnell and J.N.Hefner. AIAA, 203–261 (1990)